ACS APPLIED MATERIALS & INTERFACES

Research Article

www.acsami.org

Low-Cost, Large-Scale, and Facile Production of Si Nanowires Exhibiting Enhanced Third-Order Optical Nonlinearity

Zhipeng Huang,*[,†] Ruxue Wang,[†] Ding Jia,[†] Li Maoying,[†] Mark G. Humphrey,[‡] and Chi Zhang*[,†]

[†]Functional Molecular Materials Research Centre, Scientific Research Academy, Jiangsu University, Zhenjiang 212013, P. R. China

[‡]Research School of Chemistry, Australian National University, Canberra, ACT 0200, Australia

ABSTRACT: A facile method for the low-cost and large-scale production of silicon nanowires has been developed. Silicon powders were subjected to sequential metal plating and metal-assisted chemical etching, resulting in well-defined silicon nanowires. The morphology and structure of the silicon nanowires were investigated, revealing that single-crystal silicon nanowires with average diameters of 79 ± 35 nm and length more than 10 μm can be fabricated. The silicon nanowires show excellent third-order nonlinear optical properties, with a third-order susceptibility much larger than that of bulk silicon, porous silicon, and silicon nanocrystals embedded in SiO_2.

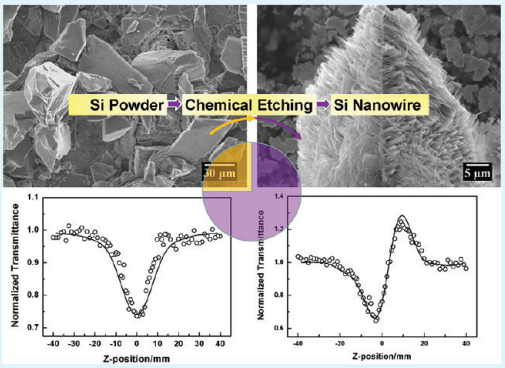

KEYWORDS: *silicon nanowire, etching, synthesis, nonlinear optics*

INTRODUCTION

Silicon (Si) nanowires are attracting considerable attention because of their promising potential in various applications ranging from biochemical or biomedical sensing,[1,2] or as field emission transistors,[3,4] to solar energy conversion[5,6] and energy storage.[7,8] Because of the fine control over the morphology and structure of Si nanowires that is possible, the mass production of Si nanowires is of especial importance for the various applications (e.g., as lithium ion batteries, solar cells and optical limiting devices). Accordingly, considerable effort has been devoted to exploit a low cost and convenient method for the mass production of Si nanowires. At present, chemical vapor deposition (CVD) approaches based on the vapor−liquid−solid mechanism,[9−12] top-down dry-etching methods (i.e., reactive ion etching, RIE[13−16]) and metal-assisted chemical etching of Si wafers[17−23] are widely utilized to fabricate Si nanowires, enabling fine control over feature size, growth orientation, orientation relative to the substrate, and the packing manner of the Si nanowires. These methods, however, rely on expensive precursors (e.g., silane in the case of CVD and SF_6 in the case of RIE) or materials (e.g., a Si substrate in the case of RIE and metal-assisted chemical etching), as well as expensive equipment in the case of CVD and RIE. Furthermore, the large-scale production of Si nanowires remains difficult, due to the unavoidable use of chambers in CVD and RIE, or the trivial procedures used for metal-assisted chemical etching. For example, to obtain isolated Si nanowires, Si nanowires generated on the surface of a wafer must be collected by mechanical scratching in metal-assisted chemical etching. This method is simple, but the extremely low output renders large-scale utilization impractical (only 20 mg of Si nanowires resulting from a 4-in. Si wafer).[24] A low-cost, convenient, and scalable production of Si nanowires remains a major challenge.

Because of the broad applications of lasers in military and civilian fields (e.g., energy weapons, optical communication, and materials processing), the protection of sensitive optical devices and human eyes is gaining considerable attention. Materials with excellent third-order nonlinear optical (NLO) capabilities exhibit considerable promise for such protection. Thus far, significant NLO properties have been found in a wide spectrum of candidate materials, including metal complexes and clusters,[25] organic materials,[26] and inorganic semiconductor nanoparticles.[27] Among these possible new materials, inorganic semiconductor nanoparticles are gaining ever-increasing attention because of their thermal stability, broad absorption bands, and abundant morphology- and composition-dependent nonlinear phenomena. It has been shown that the two-photons absorption coefficient, which defines the efficiency for one of the major mechanisms inducing nonlinear optical effects in semiconductors, increases upon decreasing the band gap of semiconductors,[28] suggesting that narrow band gap semiconductors should be promising candidates for nonlinear optical devices. Silicon is a well-known narrow band gap semiconductor, with a band gap of ca. 1.1 eV. However, the reports concerning the optical nonlinearities of Si nanowires are quite rare, with only King et al. demonstrating the nonlinear scattering of Si nanowires.[29]

Received: December 12, 2011
Accepted: February 13, 2012
Published: February 13, 2012

In this article, a facile and low-cost method for the mass production of Si nanowires is introduced, together with the preliminary investigations of their third-order nonlinear optical properties. We show that Si nanowires can be fabricated from low-cost starting materials, that the relatively simple fabrication can be accomplished in a chemistry lab under ambient atmosphere condition without recourse to expensive instrumentation, and that the resultant Si nanowires can be released from the initial materials by ultrasonication and collected by filtration. Our method is therefore a significant improvement over the previous methods, and is suitable for the large-scale production of Si nanowires. The NLO studies reveal the third order-optical nonlinearity of Si nanowires, showing their prominent nonlinear absorptive and self-focusing behavior, and demonstrating the potential of Si nanowires in the field of nonlinear optics.

EXPERIMENTAL METHODS

Chemicals. Si powders (99.99%, >400 mesh) were obtained from Sunout Energy & Material Technology Inc., China. Silver nitrate ($AgNO_3$, AR), ammonium hydroxide (AR, 30%), hydrogen peroxide (H_2O_2, 30%, GR), hydrofluoric acid (HF, 48%, GR), and nitric acid (HNO_3, 70%, AR) were purchased from Sinopharm Chemical Reagent Co., and used as received without any purification.

Fabrication of Si Nanowires. Si powders were degreased by successive 10 min ultrasonication treatments in acetone, ethanol, and deionized water. The degreased Si powders were then subjected to a boiling solution composed of $NH_3{\cdot}H_2O$ (AR, 30%), H_2O_2 (GR, 30%), and H_2O (1:1:5, v:v:v) for 30 min. The resultant hydrophilic Si powders were then rinsed with copious amount of deionized water and dried at 80 °C in an ambient atmosphere.

In a typical Ag plating experiment, hydrophilic Si powders were added to a 50 mL solution of 37.5 mL of H_2O, 12.5 mL of HF (AR, 40%), and 0.172 g of $AgNO_3$ (AR). The Ag plating proceeded under vigorous stirring at 30 °C for 30 s. One milliliter of H_2O_2 (AR, 30%) was then added dropwise into the plating solution, and Ag-loaded Si powders were catalytically etched in the $HF/H_2O_2/H_2O$ solution. The metal-assisted chemical etching was performed for a certain time, and then stopped by adding copious amount of deionized water to the etching solution. The etched Si powders were filtered through a micropore filter paper (0.2 μm), and rinsed several times with deionized water. The Ag particles loaded on the etched Si powders were removed by HNO_3 treatment (5%, 30 min). The product was then rinsed with deionized water and dried at 80 °C under an ambient atmosphere.

Morphological and Absorbance Characterization. The morphologies of the Si nanowires etched from Si powders were characterized by scanning electron microscopy (SEM, 7001F, JEOL) and transmission electron microscopy (TEM, 2100HR, JEOL). For SEM observations, Si nanowires were glued to copper plates by silver paint. For TEM characterization, the Si nanowires were dispersed in ethanol and dropped onto a carbon-coated copper grid. The specific surface area of the Si nanowires was determined from nitrogen adsorption isotherms using a nitrogen absorption/desorption analysis system (NOVA 2000, Quantachrome Inst.). The absorbance spectrum of Si nanowires was measured on a UV−vis−near IR spectrophotometer (UV 4100, Hitachi).

Nonlinear Optical Measurements. Ultrasonication in toluene released the Si nanowires from powders that had been etched for 30 min. The sediment was discarded and the Si nanowire suspension was used in third-order NLO measurements. The concentration of the Si nanowires was determined to be ca. 46 mg/L by weighing the dried sample. The third-order NLO absorptive and refractive properties of the Si nanowires were investigated by performing *Z*-scan measurements.[30] The Si nanowires were dispersed in toluene and placed in a 2 mm quartz cuvette for the nonlinear optical measurements, which were performed with linearly polarized 4 ns pulses at 532 nm generated from a Q-switched frequency-doubled Nd:YAG laser. The nanowire samples are stable toward air and laser light under the experimental conditions. The optical pulses were of a top-hat spatial profile. The pulsed laser was focused onto the sample cell with a 39.5 cm focal length mirror. The spot radius of the laser beam was measured to be 40 μm (half-width at $1/e^2$ maximum). The energy of the input and output pulses were measured simultaneously by precision laser detectors (Rjp-765a energy probes), which were linked to a computer by an IEEE interface,[30] while the incident pulse energy was varied by a Newport Com. Attenuator. The interval between the laser pulses was chosen to be 1 s to avoid the influence of thermal and long-term effects. The samples were mounted on a translation stage that was controlled by computer to move along the axis of the incident laser beam (*Z*-direction) with respect to the focal point. To determine both the sign and magnitude of the nonlinear refraction, we placed a 2 mm diameter aperture in front of the transmission detector and the transmittance recorded as a function of the sample position on the *Z*-axis (closed-aperture *Z*-scan). To measure the nonlinear absorption, we taken the *Z*-dependent sample transmittance without the aperture (open-aperture *Z*-scan).

RESULTS AND DISCUSSION

Synthesis and Characterization of Si Nanowires. Metal-assisted chemical etching is an important method to fabricate Si structures. The principle of this method is that Si in contact with a noble metal is etched much faster than Si in the absence of the noble metal, when in a mixture composed of HF and oxidant (e.g., H_2O_2). Our method is a modification of the widely utilized metal-assisted chemical etching, wherein Si powders are used as starting materials instead of Si wafers. The use of Si powder significantly reduces the cost of fabrication and increases the ease of fabrication. In brief, the approach consists of two consecutive steps (i.e., metal plating and metal-assisted chemical etching) that can be accomplished in the same plastic beaker. The surface of the Si powder is loaded with noble metal particles (e.g., Ag) by electroless metal plating (step 1, Figure 1). The Ag-loaded Si powders are then

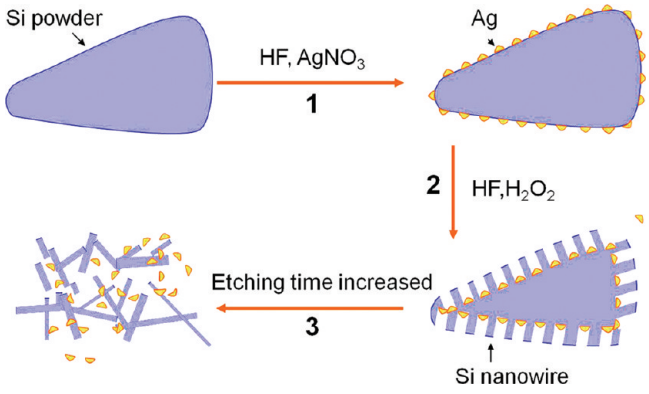

Figure 1. Illustration depicting the fabrication of Si nanowires.

subjected to an etchant composed of HF and H_2O_2. The Ag-loaded Si powders are etched into pores or wires (step 2, Figure 1). With increasing etching time, the etching depth increases, and the etched pores finally penetrate the Si powders, resulting in isolated Si nanowires (step 3, Figure 1).

Silver particles on the surface of Si particles act as microelectrodes during the metal-assisted chemical etching, dramatically enhancing the reduction of oxidant (H_2O_2) and the transfer of holes from oxidant into Si, and thereby the oxidation and then dissolution of Si. As a result, the Si below the silver particles is etched much faster than the Si remote from the Ag, and so the Si evolves into pores or wires

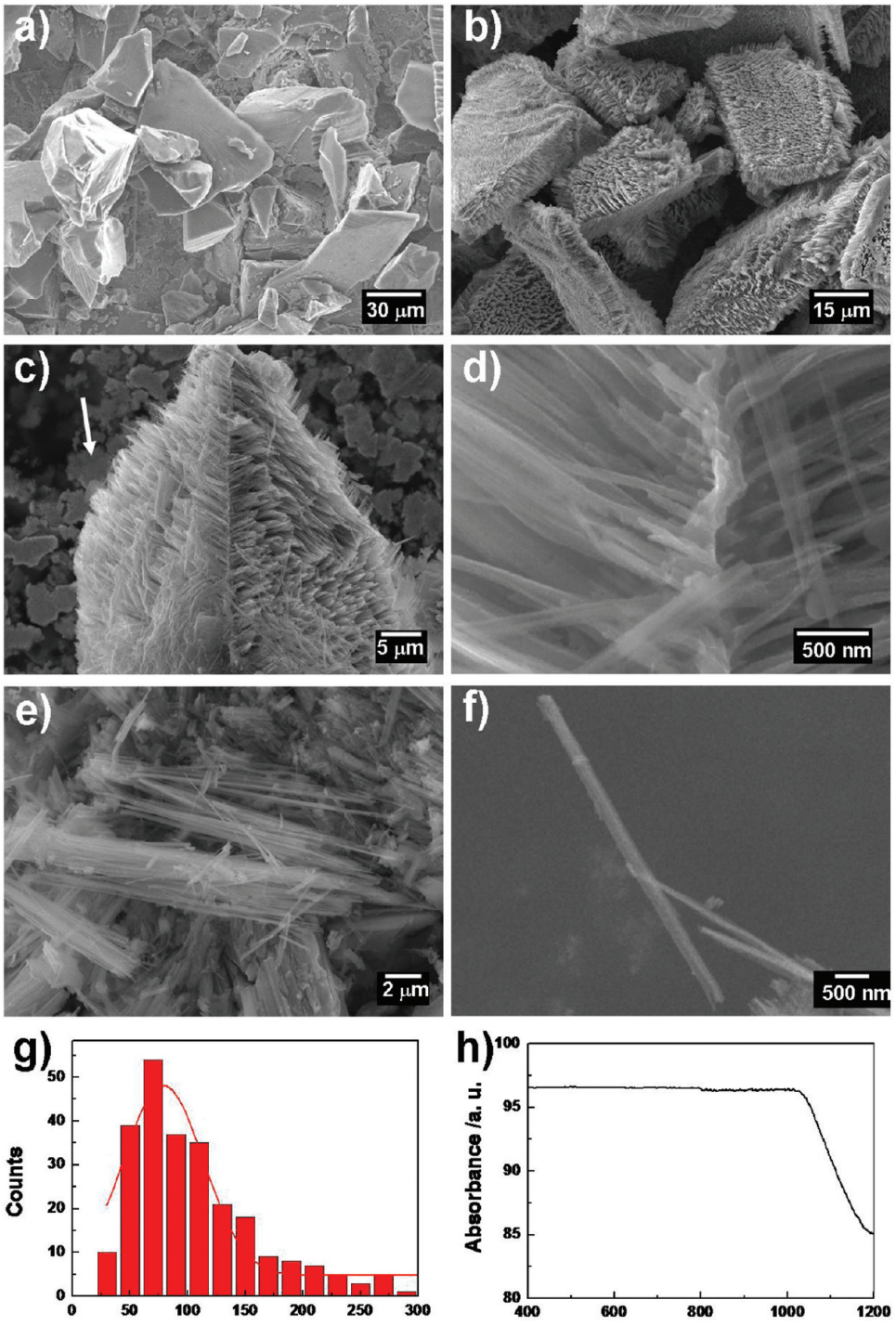

Figure 2. Low-magnification SEM images of (a) the initial Si powder and (b) the etched Si powder, with typical morphologies of products etched for (c, d) 30 min and (e, f) 60 min, respectively. Small pellets indicated by the arrow in c are Ag paint used to glue the etched Si powders onto a copper plate for the SEM characterization. (g) Diameter distribution of Si nanowires. The solid line depicts the result of corresponding Gaussian fitting, suggesting a mean diameter of 79 ± 35 nm. (h) Typical absorbance spectrum of Si nanowires.

depending on the morphologies of the silver particles and the interparticle distances. This process can be described by eq 1[23]

$$\text{cathode reaction: } H_2O_2 + 2H^+ \xrightarrow{Ag} 2H_2O + 2h^+$$

$$\text{anode reaction: } Si + 4h^+ + 4HF \xrightarrow{Ag} SiF_4 + 4H^+ \quad (1)$$

Figure 2a shows a representative SEM image of the starting Si powders. The nonetched powders exhibit irregular shapes, with a wide distribution in size ranging from several micrometers to more than 50 μm. Depending on the etching conditions, the etched structures possess two typical morphologies. If the etching time is short, the Si powders evolve into Si nanowire bundles that resemble Si pinecones (panels b–d of Figure 2). If the etching time is sufficiently long, the etched structures appear as isolated nanowires (panels e and f of Figure 2). As shown in Figure 2b, the metal-assisted chemical etching of Si powders occurs homogeneously. All facets of the Si powder

dx.doi.org/10.1021/am201758z | ACS Appl. Mater. Interfaces 2012, 4, 1553–1559

exposed to the etchant are etched into Si nanowires, and all Si powders are etched into pinecones, irrespective of their size and shape difference. Close examination of the SEM image reveals that the resulting Si nanowires are straight with diameters ranging from 30 to 300 nm, similar to those etched from polished Si wafer. The corresponding size distribution is illustrated in Figure 2g, suggesting a mean diameter of 79 ± 35 nm. The representative absorbance spectrum of Si nanowires (Figure 2h), with obvious absorption edge near 1025 nm (band gap = 1.2 eV), is similar to that of Si nanowires etched from Si wafer,[5] in accordance to the morphological similarity between Si nanowires etched from Si particles and those from Si wafer. The absorbance spectrum show a minor blue shift in comparison with that of bulk Si (band gap = 1.1 eV). The minor enlargement of band gap would be induced by the sub-100 nm diameters of Si nanowires, whereas the diameters of Si nanowires remain relatively larger than the exiton bohr diameter of Si (10 nm)[31] so that no distinct blue shift of absorbance can be observed. It is worth noting here that the Si nanowires shown in Figure 2b–d can be readily released from the Si powder by ultrasonication, with clear implications for the mass production and efficient collection of Si nanowires.

When Si powders, but not Si wafers, were used as starting material, it proved difficult to prepare a cross-sectional sample for the SEM characterization, and so it is difficult to determine the relationship between the length of etched structures (or etching rate) and the etching time. To obtain such a dependence, the productivities of samples etched for different etching times and etched in etchants with differing oxidant concentrations were measured. Because the etched pores on the Si powders are straight (Figure 2), the productivity (p) can be analytically formulated by the relation 2

$$p \equiv \frac{m_f}{m_0} = \frac{m_0 - SL\rho}{m_0} \tag{2}$$

where m_f is the weight of etched Si powder, m_0 is the weight of starting Si powder, S is the sum of the projection area of Ag particles on the surface of the Si powder, L is the depth of the etched pores (or alternatively, the length of the nanowires), and ρ is the density of Si. Therefore, the etching rate can be deduced from the productivity by eq 3

$$\upsilon \equiv \frac{L}{t} = \frac{m_0(1-p)}{S\rho t} = c\frac{1-p}{t} \tag{3}$$

where c is a constant determined by m_0, S, and ρ.

The evolution of productivity and etching rate as a function of etching time are plotted in panels a and b in Figure 3, respectively. Interestingly, the etching rate decreases gradually with etching time, which differs from the etching behavior of Si wafer in the same etchant. This difference can be attributed to the much greater surface area and the corresponding greatly increased number of reaction sites on the Si powder, in comparison with Si wafer, which induces a much faster consumption of reagents. The etching rate is kinetically determined from the concentration of HF and H_2O_2. In our experiments, the quantity of HF was far more than would be consumed by the dissolution of Si, while the amount of H_2O_2 was comparable to that needed to oxidize Si. With etching proceeding, the concentration of H_2O_2 gradually decreased, and consequently the etching rate decreased with increasing time, as seen in Figure 3b. The relation between etching rate and the concentration of H_2O_2 in the etchant can be confirmed by

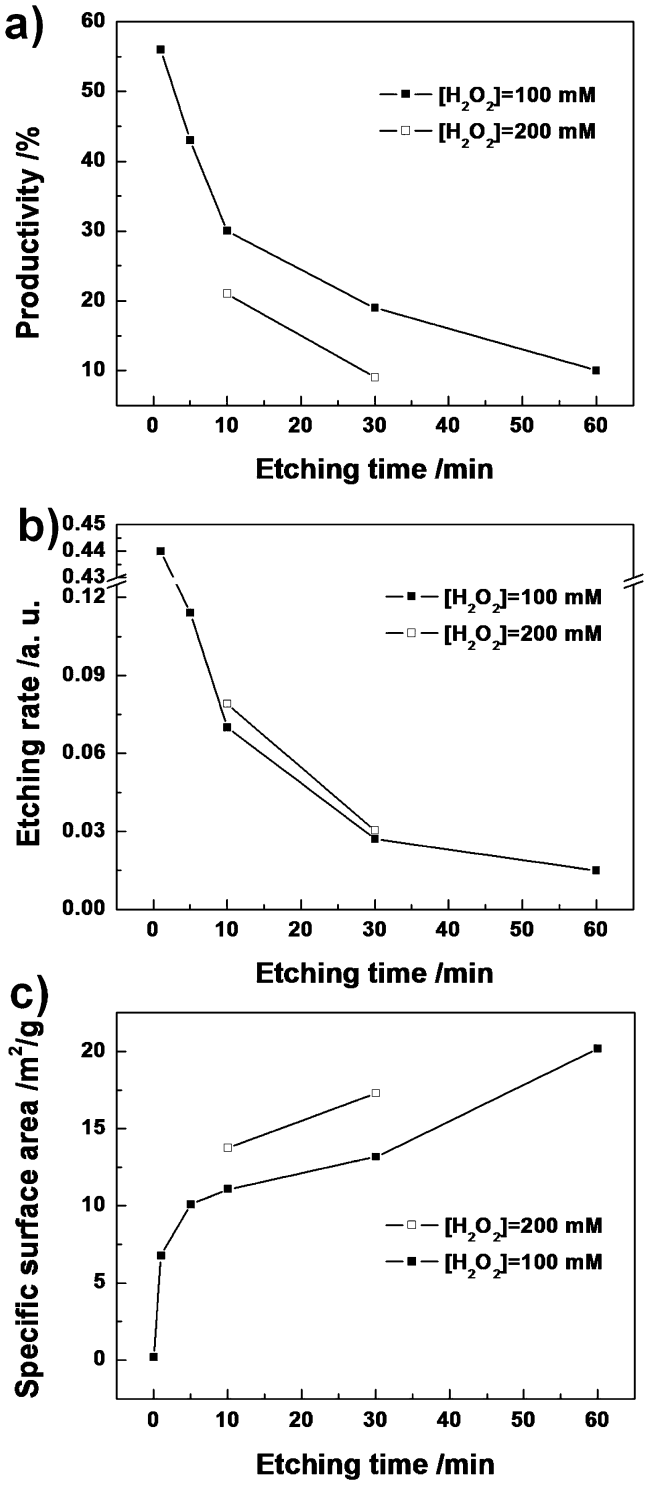

Figure 3. (a) Relation between productivity and etching time. (b) Relation between deduced etching rate and etching time. (c) Relation between specific surface area and etching time. Data for samples etched in etchant with 100 and 200 mM H_2O_2 are presented in solid and open squares, respectively.

examining productivities and etching rates of Si powders in etchants as a function of different H_2O_2 concentrations (open squares in Figure 3a, b). When the concentration of oxidant is increased from 100 mM to 200 mM, the productivity decreases from nearly 20% to less than 10%, for samples subjected to 30 min etching.

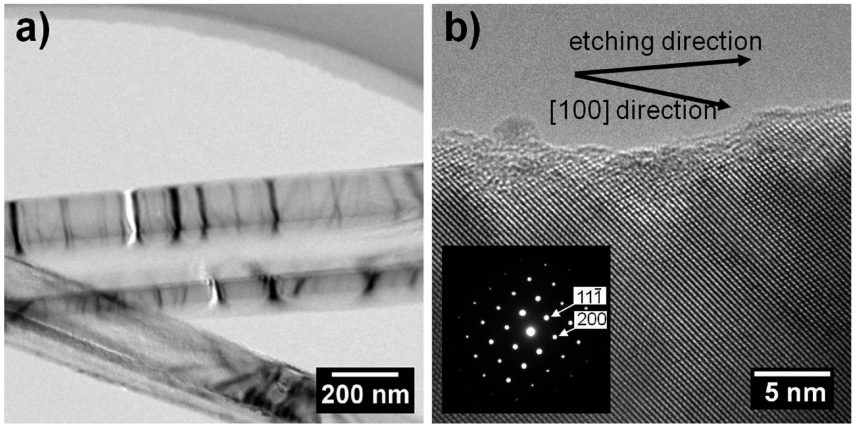

Figure 4. (a) Low-magnification and (b) high-resolution TEM images of Si nanowires etched from Si powders. The inset of b shows a [110] zone axis SAED pattern recorded from the nanowires shown in b.

The specific surface areas of samples etched for different times were measured as well, and the results are shown in Figure 3c. The specific surface area of nonetched Si powder is smaller than 0.2 m^2/g, and increases to ca. 7 m^2/g after 1 min etching. The specific surface area always increases with the etching time over the experimental time frame; however, the rate of increase first decreases with time between 1 and 30 min, and then exhibits a minor increase from 30 to 60 min. SEM characterization revealed that the typical morphologies of samples etched for 1 to 10 min are Si pinecones (Figure 2b). With the etching time increasing to 30 min, isolated Si nanowires began to appear, accompanied by the Si pinecones. After 60 min etching, most of the Si powders had evolved into isolated Si nanowires (Figure 2e). The decrease that is observed in the increasing rate of specific surface area from 5 to 30 min can therefore be attributed to the reduction of etching rate, which has been discussed above, and the subsequent increase in this increasing rate of specific surface area seen in the period from 30 to 60 min is presumably induced by the evolution of the etched Si powder from nanopinecone into isolated Si nanowires.

The crystallinity of the resultant Si nanowires was assessed by TEM. The samples were isolated nanowires, fabricated by etching the Si powder for 60 min. The low-magnification TEM image in Figure 4a suggests that the Si nanowires are single-crystalline; this conclusion is confirmed by high-resolution TEM (HRTEM) (Figure 4b), which shows the well-defined atomic lattice of Si crystal, and the corresponding [110] zone axis selected-area electron diffraction (SAED) pattern (inset of Figure 4b). The single-crystal nature of the Si nanowires is an additional benefit of the metal-assisted chemical etching method; in this method, the crystallinity of etched structures is determined by that of the starting material, because the starting material is etched under mild conditions and the etching does not induced lattice deformation or transformation of the starting material. As a result, large quantities of single-crystalline Si nanowires can be obtained by a simple etching of a relatively low-cost Si powder.

It is worth noting that the etching direction of the Si nanowires shown in Figure 4 deviates slightly from the ⟨100⟩ direction, which is the crystallographically preferred etching direction in the metal-assisted chemical etching of Si. The anisotropic etching of Si along the ⟨100⟩ direction in metal-assisted chemical etching originates from the influence of back-bond strength on the dissolution of Si atoms at the etching front. Our previous results have shown that the etching direction of non-(100) wafers is determined not only by the back-bond strength, but also by various other factors such as those restricting the movement of noble metals or affording different surface states of Si during the metal-assisted chemical etching,[21,22] and consequently the etching direction can deviate from the crystallographically preferred ⟨100⟩ direction. As shown in Figure 2a, particles in the Si powder are irregular in shape and show facets with different crystallographic orientations, including many that are non-(100).

Nonlinear Optical Studies of Si Nanowires. Si is a well-known narrow band gap semiconductor; its nanostructures are therefore promising candidates for optical limiting applications. *Z*-scan experiments were utilized to verify this possibility, with the details of the NLO measurements being described in the Experimental Section. Figure 5a displays the NLO absorptive behavior of Si nanowires and clearly shows that the absorption increases with increasing intensity of the incident laser, with the light transmittance (T) dropping to less than 75% at the focal point. The effective nonlinear absorptive coefficient (α_2) can be deduced by the fit of data from open-aperture *Z*-scan using eqs 4

$$T(z) = \frac{1}{\sqrt{\pi}\, q(z)} \int_{-\infty}^{+\infty} \ln[1 + q(z)e^{-\tau^2}]d\tau$$

$$q(z) = \int_{-\infty}^{+\infty} \int_{0}^{+\infty} \alpha_2 \frac{I_0}{1 + \left(\frac{z}{z_0}\right)^2} e^{[-2(r/\omega_0)^2 - (t/t_0)^2]} \frac{1 - e^{\alpha_0 L}}{\alpha_0} r dr dt \quad (4)$$

where light transmittance T is a function of the sample's z-position, z, with $z = 0$ defined as the focal point, τ is the temporal pulse width of the laser beam, L is the path length of the quartz cell, I_0 is the peak intensity of the laser pulse at the focus point, z_0 is defined as $z_0 = \pi\omega_0^2/\lambda$, ω_0 is the radius of the laser beam at the focus point, λ is the wavelength of the incident laser, r is the radial coordinate, t is time, t_0 is pulse width, and α_0 is the linear absorptive coefficient, respectively. A good fit between the experimental data and the theoretical curve was achieved (Figure 5a), and the nonlinear absorptive coefficient α_2 was calculated to be 3.166×10^{-10} m W^{-1}.

dx.doi.org/10.1021/am201758z | ACS Appl. Mater. Interfaces 2012, 4, 1553–1559

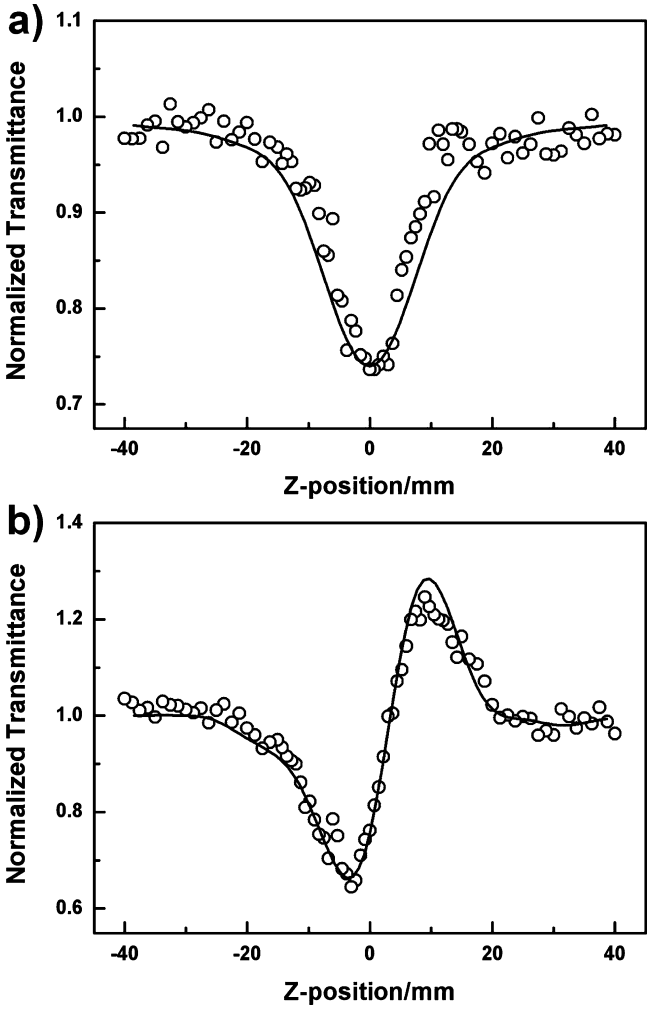

Figure 5. *Z*-scan results of Si nanowires dispersed in toluene with a linear transmittance of 85% (4 ns, 532 nm laser pulses). The half-open circles/squares represent the *Z*-scan experimental data, and the solid lines are the theoretical fitting curves: (a) data collected under the open-aperture configuration; (b) data obtained by dividing the normalized *Z*-scan data obtained under the closed-aperture configuration by the normalized *Z*-scan data in a.

The nonlinear refractive component was assessed by dividing the normalized *Z*-scan data obtained from the closed-aperture configuration by the normalized *Z*-scan data obtained from the open-aperture configuration, as depicted in Figure 5b. The valley/peak patterns of the corrected transmittance curves show an obviously self-focusing behavior of the propagating light in the Si nanowires. The effective third-order nonlinear refractive index (n_2) can be derived from the difference between the normalized transmittance values at the valley and peak positions (ΔT_{v-p}) using eq 5:

$$n_2 = \frac{\lambda\alpha_0}{0.812\pi I(1 - e^{-\alpha_0 L})}\Delta T_{v-p} \quad (5)$$

where I is the intensity of the incident laser pulse. The theoretical curves, which reproduce the general pattern of the experimentally detected data (Figure 5b), afforded the effective third-order nonlinear refractive indexes n_2 as 2.157×10^{-17} m^2 W^{-1}. On the basis of the above NLO absorptive and refractive values of these nanostructures, the modulus of the effective third-order susceptibility $\chi^{(3)}$ can be calculated to be 1.434×10^{-11} esu according to eq 6:

$$|\chi^{(3)}| = \sqrt{\left(\left|\frac{9 \times 10^8 \varepsilon_0 n_0^2 c^2}{2\upsilon}\alpha_2\right|^2 + \left|\frac{cn_0^2}{80\pi}n_2\right|^2\right)} \quad (6)$$

where υ is the frequency of the laser light, n_0 is the linear refractive index of the sample, ε_0 is the vacuum permittivity, and c is the speed of light in a vacuum.

The NLO parameters of Si nanowires can be related to the experimentally determined values according to eqs 7

$$\alpha_2 = p|f|^4\alpha_2^{Si},$$
$$n_2 - (1 - p)n_2^{sol} = p|f|^4 n_2^{Si},$$
$$\chi^{(3)} = p|f|^4\chi_{Si}^{(3)}$$
$$f = \frac{3\varepsilon_{sol}}{\varepsilon_{Si} + 2\varepsilon_{sol}} \quad (7)$$

where p is the volume fraction of Si nanowires in the solvent, f is the local field correction depending on the dielectric constant of Si nanowires (ε_{Si}) and the solvent (ε_{sol}), and n_2^{sol} is the third-order nonlinear refractive index of the solvent. With the volume fraction of Si nanowires in the solvent being ca. 2×10^{-5} and the local field correction being ca. 0.43, the NLO parameters of the Si nanowires can be extracted as $\alpha_2^{Si} = 4.697 \times 10^{-4}$ m W^{-1}, $n_2^{Si} = 6.398 \times 10^{-11}$ m^2 W^{-1}, and $\chi_{Si}^{(3)} = 4.179 \times 10^{-5}$ esu. The NLO parameters of Si nanowires presented here are 4 orders of magnitude larger than those of bulk Si,[32] porous Si,[32] and Si nanocrystals embedded in a SiO_2 matrix,[33] emphasizing the potential of Si nanowires in the field of NLO devices. The enhanced nonlinear properties of Si nanowires can be tentatively ascribed to the nonlinear scattering of Si nanowires.[29]

CONCLUSIONS

A novel and convenient approach to the low-cost, high-yielding fabrication of Si nanowires has been developed, and the dependence of nanowire length on etching time is assessed via combining weight and specific surface area measurements. Morphological and structural characterization revealed that the Si nanowires fabricated by our method are highly crystalline. *Z*-scan measurements to investigate the third-order NLO properties of the Si nanowires revealed that the Si nanowires have excellent nonlinear absorptive and refractive properties.

AUTHOR INFORMATION

Corresponding Author

*E-mail: zphuang@ujs.edu.cn; chizhang@ujs.edu.cn. Fax:86-511-8879-7815.

Notes

The authors declare no competing financial interest.

ACKNOWLEDGMENTS

This research was financially supported by the National Natural Science Foundation of China (61006049, 50925207), the Ministry of Science and Technology of China (2009DFA50620), the Ministry of Education of China (IRT1064), Six Categories of Summit Talents of Jiangsu Province, Jiangsu University (09JDG043), and the Common-

wealth of Australia under the International Science Linkages program ("Joint Research Centre for Functional Molecular Materials").

REFERENCES

(1) Cui, Y.; Wei, Q.; Park, H.; Lieber, C. M. *Science* **2001**, *293*, 1289−1292.
(2) Patolsky, F.; Zheng, G.; Lieber, C. M. *Nat. Protocols* **2006**, *1*, 1711−1724.
(3) Goldberger, J.; Hochbaum, A. I.; Fan, R.; Yang, P. *Nano Lett.* **2006**, *6*, 973−977.
(4) Schmidt, V.; Riel, H.; Senz, S.; Karg, S.; Riess, W.; Gösele, U. *Small* **2006**, *2*, 85−88.
(5) Peng, K. Q.; Xu, Y.; Wu, Y.; Yan, Y. J.; Lee, S. T.; Zhu, J. *Small* **2005**, *1*, 1062−1067.
(6) Peng, K. Q.; Lee, S. T. *Adv. Mater.* **2011**, *23*, 198−215.
(7) Chan, C. K.; Peng, H.; Liu, G.; McIlwrath, K.; Zhang, X. F.; Huggins, R. A.; Cui, Y. *Nat. Nanotechnol.* **2008**, *3*, 31−35.
(8) Peng, K.; Jie, J.; Zhang, W.; Lee, S. T. *Appl. Phys. Lett.* **2008**, *93*, 033105.
(9) Wagner, R. S.; Ellis, W. C. *Appl. Phys. Lett.* **1964**, *4*, 89−90.
(10) Hochbaum, A. I.; Fan, R.; He, R. R.; Yang, P. D. *Nano Lett.* **2005**, *5*, 457−460.
(11) Wu, Y. Y.; Fan, R.; Yang, P. D. *Nano Lett.* **2002**, *2*, 83−86.
(12) Schmidt, V.; Wittemann, J. V.; Senz, S.; Gosele, U. *Adv. Mater.* **2009**, *21*, 2681−2702.
(13) Hsu, C. M.; Connor, S. T.; Tang, M. X.; Cui, Y. *Appl. Phys. Lett.* **2008**, *93*, 133109.
(14) Morton, K. J.; Nieberg, G.; Bai, S. F.; Chou, S. Y. *Nanotechnology* **2008**, *19*, 345301.
(15) Zschech, D.; Kim, D. H.; Milenin, A. P.; Scholz, R.; Hillebrand, R.; Hawker, C. J.; Russell, T. P.; Steinhart, M.; Gosele, U. *Nano Lett.* **2007**, *7*, 1516−1520.
(16) Beckman, R. A.; Johnston-Halperin, E.; Melosh, N. A.; Luo, Y.; Green, J. E.; Heath, J. R. *J. Appl. Phys.* **2004**, *96*, 5921−5923.
(17) Peng, K. Q.; Yan, Y. J.; Gao, S. P.; Zhu, J. *Adv. Mater.* **2002**, *14*, 1164−1167.
(18) Peng, K. Q.; Wu, Y.; Fang, H.; Zhong, X. Y.; Xu, Y.; Zhu, J. *Angew. Chem., Int. Ed.* **2005**, *44*, 2737−2742.
(19) Huang, Z. P.; Fang, H.; Zhu, J. *Adv. Mater.* **2007**, *19*, 744−748.
(20) Huang, Z. P.; Zhang, X. X.; Reiche, M.; Liu, L. F.; Lee, W.; Shimizu, T.; Senz, S.; Gösele, U. *Nano Lett.* **2008**, *8*, 3046−3051.
(21) Huang, Z. P.; Shimizu, T.; Senz, S.; Zhang, Z.; Zhang, X. X.; Lee, W.; Geyer, N.; Gösele, U. *Nano Lett.* **2009**, *9*, 2519−2525.
(22) Huang, Z. P.; Shimizu, T.; Senz, S.; Zhang, Z.; Geyer, N.; Gösele, U. *J. Phys. Chem. C* **2010**, *111*, 10683−10690.
(23) Huang, Z. P.; Geyer, N.; Werner, P.; Boor, J. d.; Gösele, U. *Adv. Mater.* **2011**, *23*, 285−308.
(24) Duan, X. F.; Qu, Y. Q.; Zhong, X.; Li, Y. J.; Liao, L.; Huang, Y. *J Mater. Chem.* **2010**, *20*, 3590−3594.
(25) Zhang, C.; Song, Y. L.; Wang, X. *Coord. Chem. Rev.* **2007**, *251*, 111−141.
(26) Spangler, C. W. *J. Mater. Chem.* **1999**, *9*, 2013−2020.
(27) Wang, J.; Blau, W. J. *J. Opt. A−Pure Appl. Op.* **2009**, *11*, 024001.
(28) Eric, W.; Van Strylan; Woodall, M. A.; Vanherzeele, H.; Soileau, M. J. *Opt. Lett.* **1985**, *10*, 490−492.
(29) King, S. M.; Chaure, S.; Doyle, J.; Colli, A.; Ferrari, A. C.; Blau, W. J. *Opt. Commun.* **2007**, *276*, 305−309.
(30) Sheik-Bahae, M.; Said, A. A.; Wei, T. H.; Hagan, D. J.; Van Stryland, E. W. *IEEE J. Quantum Electron.* **1990**, *26*, 760−769.
(31) Canham, L. T. *Appl. Phys. Lett.* **1990**, *57*, 1046−1048.
(32) Henari, F. Z.; K., M.; Blau, W. J.; A., K. V.; Dneprovskii, V. S. *Appl. Phys. Lett.* **1995**, *63*, 323−325.
(33) Prakash, G. V.; Cazzanelli, M.; Gaburro, Z.; Pavesi, L.; Iacona, F.; Franzò, G.; Priolo, F. *J. Appl. Phys.* **2002**, *91*, 4607−4610.